(Article begins on next page)

Model-Based Image Reconstruction for Linear Array Optoacoustic Imaging

Roberto M. Scardigno
Department of Electrical and Information Engineering
Polytechnic University of Bari
Bari, Italy
r.scardigno1@phd.poliba.it

Antonio Brunetti
Department of Electrical and Information Engineering
Polytechnic University of Bari
Bari, Italy
antonio.brunetti@poliba.it

Silvia Seoni
Biolab, Polito[BIO]Med Lab, Department of Electronics and Telecommunications
Politecnico di Torino
Torino, Italy
silvia.seoni@polito.it

Domenico Buongiorno*
Department of Electrical and Information Engineering Polytechnic University of Bari
Bari, Italy
domenico.buongiorno@poliba.it

Kristen M. Meiburger*
Biolab, Polito[BIO]Med Lab, Department of Electronics and Telecommunications
Politecnico di Torino
Torino, Italy
kristen.meiburger@polito.it

Christoph Dehner
iThera Medical GmbH
Munich, Germany
christoph.dehner@ithera-medical.com

Guillaume Zahnd*
iThera Medical GmbH
Munich, Germany
guillaume.zahnd@ithera-medical.com

*These authors contributed equally

***Abstract*— Optoacoustic imaging is a promising biomedical imaging technique that combines optical contrast with ultrasonic resolution by detecting acoustic waves generated from pulsed light absorption in tissues. Two main issues with optoacoustic imaging are image reconstruction algorithms and the impact of probe geometry. Traditional reconstruction methods offer reasonable image quality but struggle with physical limitations; hence model-based (MB) reconstruction methods that incorporate complex tissue properties have been explored. Linear ultrasound probes are affordable and easy to manufacture, but they suffer from limited-view artifacts that degrade image quality. Concave probes, with better angular coverage, provide higher image quality but are more expensive and complex to manufacture. This study compares MB reconstruction using linear and concave probes across in-silico, in-vitro, and in-vivo images. The results show that regularized MB reconstruction can significantly enhance the quality of images obtained with linear probes, reducing the performance gap with concave arrays. For Shearlet L1 regularization, the structural similarity index (SSIM) was 0.66 ± 0.06, and the mean absolute error (MAE) was 0.057 ± 0.017, and a qualitative analysis revealed fewer artifacts in MB-reconstructed images when compared to traditional methods. Future work will focus on larger datasets and exploring deep learning to further improve MB reconstruction for linear arrays.**

Keywords—optoacoustics, photoacoustics, image reconstruction, model-based, linear array

This study was carried out within the "Development of inclusive quantitative photoacoustic imaging solutions enabled by ethical artificial intelligence (ImPACT-AI)" project, funded by European Union – Next Generation EU within the PRIN 2022 PNRR program (D.D.1409 del 14/09/2022 Ministero dell'Università e della Ricerca). This manuscript reflects only the authors' views and opinions, and the Ministry cannot be considered responsible for them.

This study was partially founded by the European Union – Next Generation Eu - under the National Recovery and Resilience Plan (NRRP), Mission 4 Component 2 Investment 3.3 - Decree No. 351 (09th April 2022) of Italian Ministry of University and Research - Concession Decree No. 2153 (28th December 2022) of the Italian Ministry of University and Research, Project code D93D22001390001, within the Italian National Program PhD Programme in Autonomous Systems (DAuSy).

I. Introduction

Optoacoustic imaging is an emerging biomedical imaging modality that combines the advantages of both optical contrast and ultrasonic resolution, by detecting acoustic waves that are generated by the absorption of pulsed light within the tissue [1]. Traditional optoacoustic image reconstruction techniques, such as delay-and-sum beamforming and time-reversal methods, are typically employed and can provide reasonable image quality; however, they suffer from theoretical limitations, such as the inability to accurately account for heterogeneous acoustic properties and the need for a constant speed of sound assumption [2].

To overcome some of these challenges, model-based (MB) optoacoustic image reconstruction approaches have been explored. These techniques rely on accurate forward models of the optoacoustic wave propagation, which can incorporate the complex acoustic properties of the tissue [3]. By incorporating these models into iterative reconstruction algorithms, it is possible to partially compensate for the effects of heterogeneous acoustic properties and generally improve the overall image quality [4].

Additionally, the use of linear ultrasound probes can provide a practical solution for optoacoustic imaging

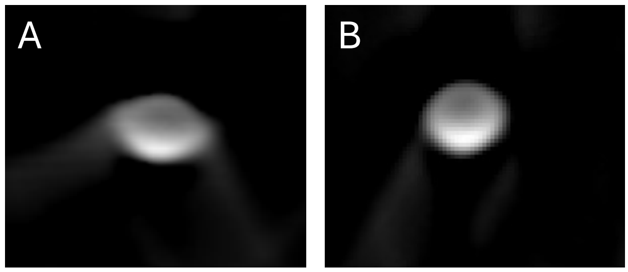

Fig. 1. Qualitative example displaying image quality differences, in terms of limited-view artifacts, for a linear probe (A) and a concave probe (B) on a simple in-silico image.

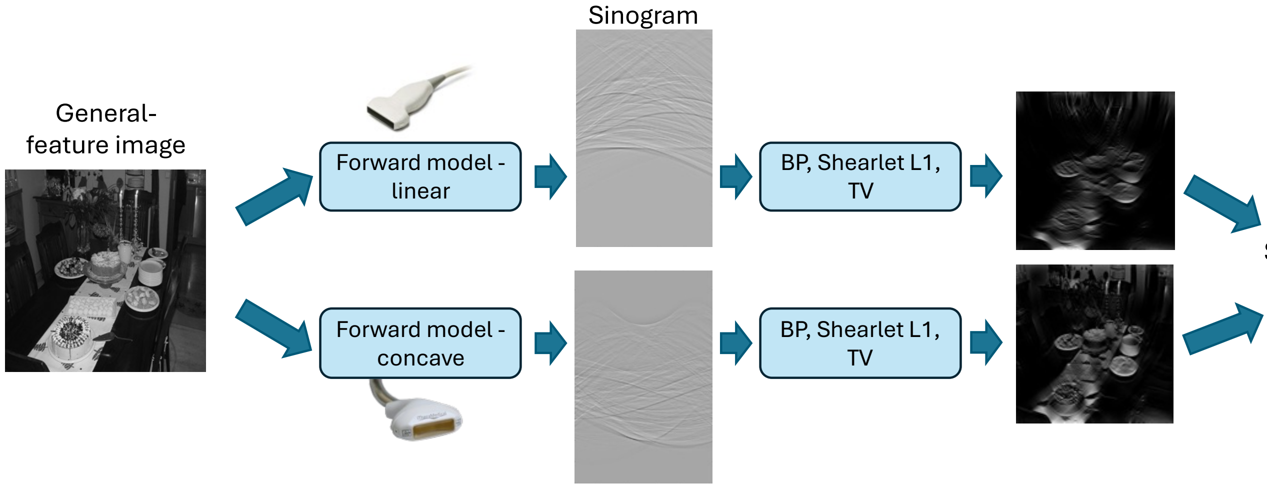

Fig. 2. Pipeline of the work presented.

applications. Linear probes are simple and inexpensive to manufacture; however, the limited view geometry associated with linear probes can introduce reconstruction limited-view artifacts, which lower the overall image quality [5]. Concave arrays can overcome some of these limited-view artifacts by providing a higher angular coverage, but are typically more complex and expensive to manufacture. A qualitative example of how the probe geometry can influence image quality is shown in Fig. 1.

The combination of model-based reconstruction methods and the use of linear ultrasound probes holds promise for overcoming some of these limitations in optoacoustic imaging and here we aim to generalize the implementation of MB reconstruction methods with regularization to a common linear array geometry and compare the results with those obtained using a concave array (125° angular coverage).

II. Materials and Methods

Fig. 2 shows the pipeline that was employed and the following subsections describe in detail the dataset, the model-based reconstruction methods that were implemented, and the validation metrics.

A. Dataset description

Three different datasets were adopted to validate and test the compared methods: a simulated, an in-vitro, and an in-vivo dataset. The simulated dataset was obtained by randomly selecting 256 images from the VOC2012 public dataset [6]. The images were processed through a forward model to compute the sinograms, simulating the acquisition with both the concave and the linear probes, thus allowing for a direct comparison between the reconstruction performance.

The two probes differ only for the transducers geometry and exhibit the following characteristics: a central frequency of 4 MHz, 256 transducers, and the Field of View (FOV) equal to x:[−0.2;0.2]; y:[−0.2;0.2].

A simple customized phantom of agar with pencil leads was used to obtain in-vitro acquisitions. The acquisitions were obtained using the Verasonics Vantage 256 with a 7.5 MHz linear array (L11-5v) coupled with an Opotek Phocus Mobile SE pulsed laser. Unlike the probe used for the simulated sinograms, the L11-5v linear probe is composed of 128 transducers.

The in-vivo images were acquired by placing the probe on a human forearm and using the same hardware used for in-vitro acquisitions.

B. Image reconstruction

Here, we describe the methodologies used to reconstruct the PA images using simulated or acquired sinograms. Two methods have been compared: the backprojection and the model-based reconstruction with two regularization techniques: the L1-Shearlet and the Total Variation (TV) regularization. The work was developed on Matlab, using the MSOT Model-based Reconstruction Toolbox [7], [8].

1) Backprojection reconstruction: The backprojection method allows for real-time reconstruction, since it is computationally lightweight, although it generates several types of artifacts. A spherical integral models detector measurements and, under simplifications, relates to inverting the spherical mean Radon transform. By calculating pixel-detector distances and converting travel times into indices, the image is reconstructed using the backprojection formula:

$$p_{0_{rec}}(x,y)=\sum_{i=1}^{n} S_i(T)[R\text{-}x\cos(\Theta_i)\text{-}y\cos(\Theta_i)]dtc$$

where $p_{0_{rec}}(x,y)$ is the reconstructed image, i is the i-th transducer in the array, $S_i(T)$ is the signal of i-th transducer and depend on the travel time of the signal from each pixel to each transducer, Θ_i is the angular position of each transducer and c is the speed of sound value.

2) Model-based reconstruction: To overcome the disadvantages of backprojection reconstruction, model-based methods have been deeply investigated. To date, this method represents the state-of-the-art in PA image reconstruction, since it produces fewer artifacts, but at the expense of a high computational expense. This kind of reconstruction allows to incorporate prior knowledge about the acquisition system, such as the impulse response of the specific probe [9]. The MB reconstruction is performed through iterative steps, i.e., for this work the number of steps has been set to 200, using a realistic Electric Impulse Response. For both simulated and in-vitro datasets, the regularization parameters have been fine-tuned using the L-curve method, which compares the norm of a regularized solution versus the norm of the corresponding residual norm.

C. *Validation parameters*

In this section the metrics used to compare the performance of the linear probe with respect to the concave probe are presented. Two pixel-based metrics were adopted: the Structural Similarity Index Measure (SSIM) and the Mean Absolute Error (MAE).

1) SSIM: The SSIM is a perceptual metric that compares two images based on structural information, luminance, and contrast, making it more aligned with human visual perception than simple pixel-wise comparisons. The SSIM value ranges from -1 to 1, where 1 indicates perfect similarity, 0 indicates no similarity, and -1 indicates perfect anti-correlation.

2) MAE: The MAE is a statistical measure that calculates the average absolute difference between the intensity values of corresponding pixels in two images. It evaluates the pixel-wise differences without considering structural or perceptual factors. A lower MAE value indicates a closer match between the images.

III. Results

A. *L-curve results*

Fig. 3 displays an example aggregated L-curve plot obtained on the in-silico images that represents the relationship between the norm of the residual and the norm of the regularization term for the regularization parameters lambda for model-based reconstruction using Shearlet L1 regularization.

As can be seen, the L-curve shows a distinct inflection point: the chosen parameter that should minimize both the error in fitting and excessive smoothing was chosen to be equal to lambda = 1e-5. For the model-based reconstruction with TV regularization, a similar L-curve analysis was done and the inflection point was found for lambda equal to 1e-4.

B. *Qualitative and quantitative results*

Table I shows the quantitative SSIM and MAE results obtained for the different reconstruction methods comparing the image obtained with a concave probe geometry with the image obtained with a linear probe geometry.

Regularized MB reconstruction can close the gap between linear and concave arrays: the SSIM and MAE was 0.66 ± 0.06 and 0.057 ± 0.017, respectively, for L1 Shearlet, and 0.62 ± 0.05 and 0.068 ± 0.019, respectively, for TV. Regularized MB reconstruction of scans acquired with a linear array are markedly superior to those reconstructed with BP, as can also be qualitatively appreciated in Fig. 4. The first two rows of this figure display two general feature images that were employed for L-curve analysis and for which we have a one-to-one comparison between the images obtained using a concave probe geometry and a linear probe geometry (i.e., it is possible to compute the SSIM and MAE validation metrics).

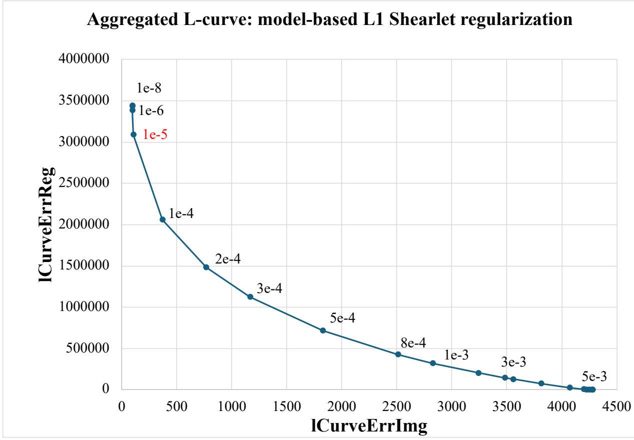

Fig. 3. Example aggregated L-curve for in-silico images for model-based reconstruction with Shearlet L1 regularization. The inflection point can be seen for lambda = 1e-5.

To test whether the MB reconstruction with regularization can also close the gap in a practical setting, a phantom image of lead within agar and an in-vivo image of the forearm of a healthy volunteer were acquired using the Verasonics Vantage 256 ultrasound research platform coupled with the Opotek Phocus Mobile SE pulsed laser. A linear array (L11-5v) with a central frequency of 7.5 MHz was employed for image acquisition. The raw data were then given as input to the MB and BP reconstruction algorithms, employing the same parameters as described previously. Qualitative results are shown in the last two rows of Fig. 4.

TABLE I. Quantitative results comparing images reconstructed using concave and linear probe geometries

Reconstruction method	**Validation parameter**	
	Structural Similarity Index Measure (SSIM)	***Mean Absolute Error (MAE)***
Backprojection	0.732 ± 0.060	0.013 ± 0.003
L1 Shearlet	0.662 ± 0.056	0.057 ± 0.017
Total Variation	0.618 ± 0.050	0.068 ± 0.019

IV. Discussion and Conclusions

Regularized MB reconstruction can improve the quality of linear array images and stay close to the quality of concave array images, as the quantitative SSIM and MAE validation parameters shown in Table I demonstrate. Here it is important to point out that it appears that the best SSIM (i.e., the highest value) and the best MAE (i.e., the lowest value) were obtained for the simple backprojection image reconstruction algorithm and not for the model-based reconstruction algorithms. However, the considered paired metrics (i.e., SSIM and MAE) do not take into account the initial quality of the reconstructed images, but rather simply compare the image reconstructed with the concave probe geometry with the image reconstructed with the linear probe geometry. Hence, if the quality of the backprojection reconstruction method is low, but similar results are obtained with the two different probe geometries, the metrics will be optimal. Therefore, it is important to couple these quantitative metrics also with a

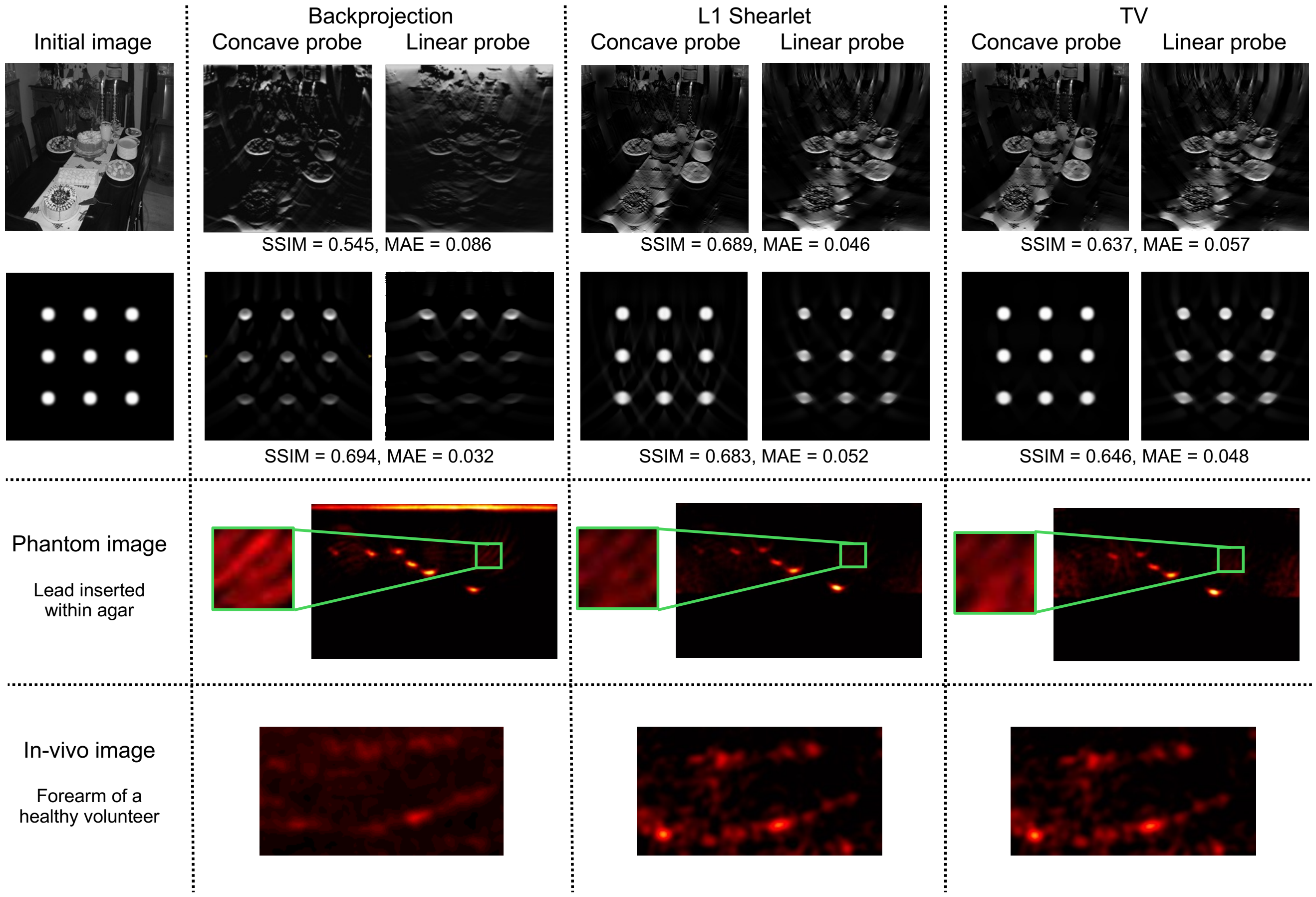

Fig. 4. Qualitative and quantitative examples displaying image quality differences for the three reconstruction methods employed (i.e., backprojection, Shearlet L1, and Total Variation). The bottom two rows show the qualitative results obtained on an in-vitro phantom image and an in-vivo image of the forearm of a healthy volunteer.

qualitative visual analysis, which clearly portrays how the regularized MB reconstruction of scans acquired with a linear array are markedly superior to those reconstructed with BP. This shows promise for obtaining images with a quality similar to those reconstructed with concave arrays covering a larger angular coverage. In fact, regularized MB reconstructed images showed reduced limited-view artifacts not only in the in-silico images but also in both in-vitro and in-vivo experimental images.

We present here an initial study using a limited dataset. Future work will focus on extending the analysis to a larger dataset, which could likely include further optimization of model-based regularization terms. Importantly, we plan on expanding the in-vitro and in-vivo datasets, to further demonstrate the applicability and generalizability of the method to more complex optoacoustic images. Finally, this work could be an important first step for exploring the use of deep learning-based methods to generalize regularized MB reconstruction algorithms for linear probe arrays [10].

References

[1] Beard P., 2011. Biomedical photoacoustic imaging. *Interface focus*, *1*(4), pp.602-631.

[2] Lutzweiler C. and Razansky D., 2013. Optoacoustic imaging and tomography: reconstruction approaches and outstanding challenges in image performance and quantification. *Sensors*, *13*(6), pp.7345-7384.

[3] Dean-Ben X.L., Ntziachristos V. and Razansky D., 2012. Acceleration of optoacoustic model-based reconstruction using angular image discretization. *IEEE Transactions on medical imaging*, *31*(5), pp.1154-1162.

[4] Dean-Ben X.L. and Razansky D., 2022. A practical guide for model-based reconstruction in optoacoustic imaging. *Frontiers in Physics*, *10*, p.1028258.

[5] Deán-Ben X.L. and Razansky D., 2016. On the link between the speckle free nature of optoacoustics and visibility of structures in limited-view tomography. *Photoacoustics*, *4*(4), pp.133-140.

[6] Everingham, M., Van Gool, L., Williams, C. K. I., Winn, J., & Zisserman, A.. The PASCAL Visual Object Classes Challenge 2012 (VOC2012) Results [Dataset]. http://www.pascal-network.org/challenges/VOC/voc2012/workshop/index.html

[7] Chowdhury K.B., Prakash J., Karlas A., Jüstel D., and Ntziachristos V. A synthetic total impulse response characterization method for correction of hand-held optoacoustic images. IEEE Transactions on Medical Imaging, 39(10):3218-30, 2020.

[8] Chowdhury K.B., Bader M., Dehner C., Jüstel D., and Ntziachristos V. Individual transducer impulse response characterization method to improve image quality of array-based handheld optoacoustic tomography. Optics Letters 46(1):1-4, 2021.

[9] Chowdhury K. B., Prakash J., Karlas A., Jüstel D. and Ntziachristos V., "A Synthetic Total Impulse Response Characterization Method for Correction of Hand-Held Optoacoustic Images," in IEEE Transactions on Medical Imaging, vol. 39, no. 10, pp. 3218-3230, Oct. 2020, doi: 10.1109/TMI.2020.2989236.

[10] Dehner C., Zahnd G., Ntziachristos V., & Jüstel D. (2023). A deep neural network for real-time optoacoustic image reconstruction with adjustable speed of sound. *Nature Machine Intelligence*, *5*(10), 1130-1141.